

Searches for stochastic gravitational-wave backgrounds

Joseph D. Romano

Les Houches Summer School
July 2018

Abstract

These lecture notes provide a brief introduction to detection methods used to search for a stochastic background of gravitational radiation—i.e., a superposition of gravitational-wave signals either too weak or too numerous to individually detect. The lectures are divided into two main pieces: (i) an overview, consisting of a description of different types of gravitational-wave backgrounds and an introduction to the correlation method using multiple detectors; (ii) details, extending the previous discussion to non-trivial detector response, what to do in the absence of correlations, and a recently proposed Bayesian method to search for the gravitational-wave background produced by stellar-mass binary black hole mergers throughout the universe. Suggested exercises for the reader are given throughout the text.

Contents

1 Motivation	3
1.1 Gravitational-wave analogue of the CMB	3
1.2 The background of BBH and BNS mergers in the LIGO band	4
2 Different types of stochastic backgrounds	5
2.1 Different sources	5
2.2 Different signal properties	6
3 Mathematical characterization of a stochastic background	9
3.1 Ensemble averages and the energy density spectrum in GWs	9
3.2 Calculating $\Omega_{\text{gw}}(f)$ for an astrophysically-generated background	11
4 Correlation methods - basic idea	11
5 Some simple examples	11
6 Non-trivial detector response	11
7 Non-trivial correlations	11
8 What to do in the absence of correlations?	11
9 Searching for the background of binary black-hole mergers	11
10 Exercises	12

1 Motivation

A stochastic background of gravitational radiation is a superposition of gravitational-wave signals either too weak or too numerous to individually detect. The individual signals making up the background are thus *unresolvable*, unlike the large signal-to-noise binary black-hole (BBH) and binary neutron-star (BNS) merger signals recently detected by the advanced LIGO and Virgo detectors. But despite the fact that the individual signals are unresolvable, the detection of a stochastic gravitational-wave background (GWB) will be able to provide information about the *statistical* properties of the source.

1.1 Gravitational-wave analogue of the CMB

The ultimate goal of gravitational-wave background searches is to produce the GW equivalent of Figure 1, which is a sky map of the temperature fluctuations in the CMB blackbody radiation,

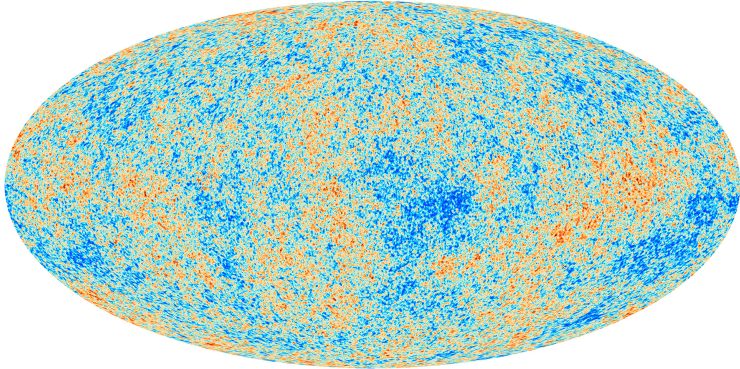


Figure 1: Skymap of $\Delta T/T_0$ for the cosmic microwave background radiation produced by the Planck 2013 mission.

$\Delta T/T$, relative to the $T_0 = 2.73$ K isotropic component. (The dipole contribution due to our motion with respect to the cosmic rest frame has also been subtracted out.) Recall that the CMB is a background of electromagnetic radiation, produced at the time of last scattering, roughly 380,000 yr after the Big Bang. At that time, the universe had a temperature of ~ 3000 K, approximately one thousand times larger than the temperature today, but cool enough for neutral hydrogen atoms to first form and photons to propagate freely. The temperature fluctuations in the CMB radiation tell us about the density of matter on the surface of last scattering, thus giving us a picture of the “seeds” of large-scale structure formation in the early universe. Given the weakness of the gravitational interaction compared to the electromagnetic force, the GW equivalent of Figure 1 would give us a picture of the Universe a mere fraction of a second after the Big Bang (this is explained in a bit more detail in Section 2.1)—a “holy grail” for gravitational-wave astronomy.

For perspective, Figure 1 was produced by the Planck mission in 2013, almost 50 years after the CMB radiation was initially detected by Penzias and Wilson in 1965. It took many years and improved experiments (COBE, Boomerang, WMAP, Planck to name a few) to get to the high-precision measurements that we have today. So it is somewhat sobering to realize that now—at the end of 2018—we have yet to detect the isotropic component of the GWB.

1.2 The background of BBH and BNS mergers in the LIGO band

But fortunately, as mentioned above, the advanced LIGO and Virgo detectors have detected other gravitational-wave signals from several individual BBH and BNS mergers. These were very strong signals, having matched-filter signal-to-noise ratios $\text{SNR} \gtrsim 10$, and false alarm probabilities $< 2 \times 10^{-7}$, corresponding to 5-sigma “gold-plated” events. Similar large SNR detections are expected during the upcoming observing run O3, which is scheduled to start in early 2019. But we also expect that there are many more signals, corresponding to more distant mergers or smaller mass systems, which are individually undetectable (i.e., *subthreshold* events). This weaker background of gravitational radiation is nonetheless detectable *as a collectivity* via the common influence of the gravitational waves on multiple detectors.

To get an idea of the statistical properties of this background signal, we can estimate the total rate of stellar-mass BBH mergers throughout the universe by using the local rate estimate from these first detections, $9\text{--}240 \text{ Gpc}^{-3} \text{ yr}^{-1}$. This leads to a prediction for the total rate of BBH mergers between ~ 1 per minute to a few per hour. (*Exercise: 1:* Verify these values for the total rate.¹) Since the duration of BBH merger signals in band is ~ 1 s, which is much smaller than the average duration between successive mergers, the combined signal will be highly-nonstationary (or *popcorn-like*). We can perform similar calculations for BNS mergers. The predicted total rate for such events is roughly one event every 15 s, while the duration of a BNS signal in band is roughly 100 s. Thus, the BNS merger signals overlap in time leading to a continuous (or *confusion-limited*) background. Figure 2 is a plot of the expected time-domain signal corresponding the rate estimates calculated above.

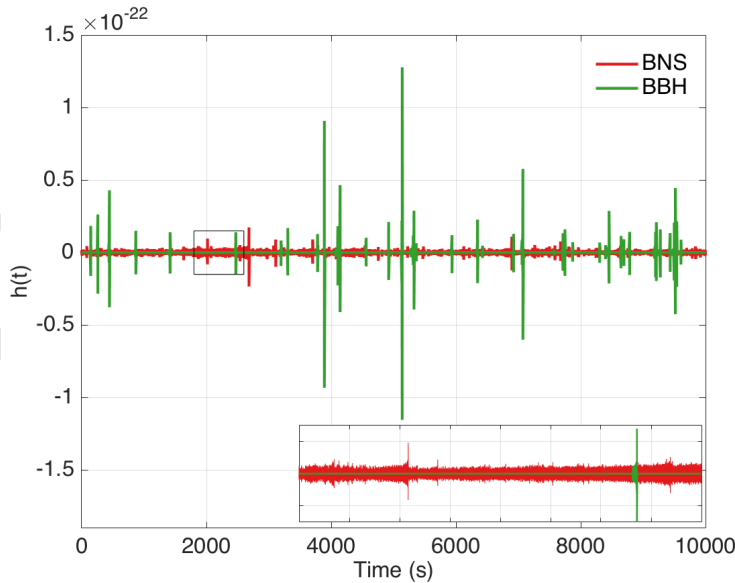


Figure 2: Simulated time-domain signal for the predicted BBH and BNS background. Figure taken from [?].

The combined signal from BBH and BNS mergers is potentially detectable with advanced LIGO and Virgo, shortly after reaching design sensitivity. Although the signal-to-noise ratios for the individual events are small, the combined signal-to-noise ratio of the correlated data summed

¹A more complete description of this and all other exercises is given in Section 10.

over all events grows like the square-root of the observation time, reaching a detectable level of 3-sigma after roughly 40 months of observation (Figure 3). This estimate of time to detection is

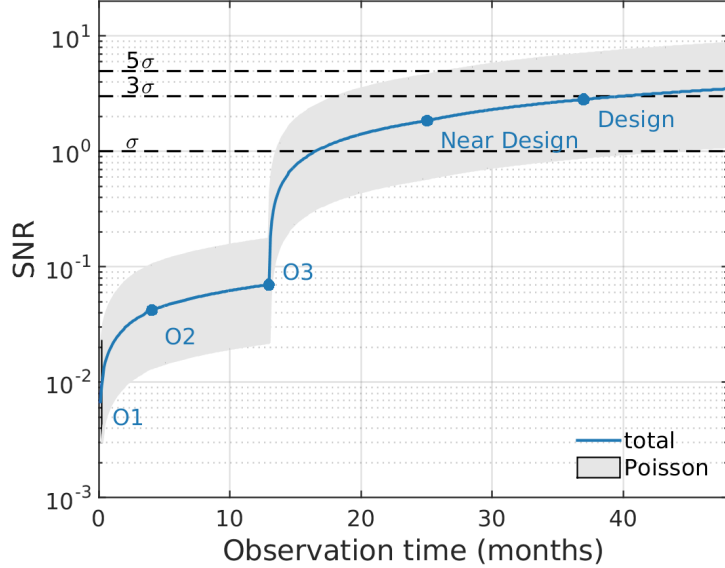


Figure 3: Expected signal-to-noise ratio of the correlated data for the advanced LIGO and Virgo detectors as a function of observation time. The points labeled O1, O2, etc., indicate the start of advanced LIGO’s first observation run, second observation run, etc. Figure taken from [?].

based on the standard cross-correlation search (Section 4), which assumes a Gaussian-stationary background. But there is a better method, recently proposed by Smith and Thrane [2], which should reduce the time to detection by several orders of magnitude (factor of ~ 1000), meaning that the background would be detectable after only a few days of operation. We will describe this method in more detail in Section 9.

2 Different types of stochastic backgrounds

2.1 Different sources

The combined signal from stellar-mass BBH and BNS mergers throughout the universe is just one way of producing a GWB. Due to the relatively small masses of stellar-mass BHs and NSs, the signal is at the high-frequency end of the spectrum (~ 10 Hz to a few kHz), which is the sensitive band for the current generation of km-scale ground-based laser interferometers like LIGO and Virgo. Heavier-mass systems, which produce lower-frequency gravitational waves, are also expected to give rise to GWBs that are potentially detectable with other existing or proposed detectors. Figure 5 is a plot of the gravitational-wave spectrum, with frequencies ranging from a few kHz (for ground-based detectors) to 10^{-17} Hz (corresponding to a period equal to the age of the universe), together with potential sources of GWBs and relevant detectors.

Of particular note is the combined gravitational-wave signal produced by compact white-dwarf binaries in the Milky Way, producing a “confusion-limited” GWB in the frequency band $\sim 10^{-4}$ Hz to 10^{-1} Hz. This is a guaranteed signal for the proposed space-based interferometer LISA, which consists of three spacecraft (each housing two lasers, two telescopes, and two test masses) in an

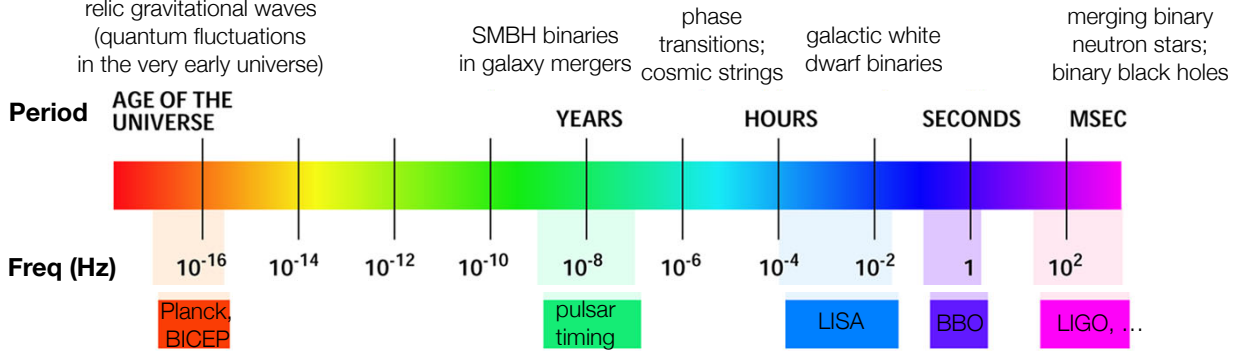


Figure 4: Detectors and potential sources of gravitational-wave backgrounds across the gravitational-wave spectrum.

equilateral-triangle configuration (arm lengths of several million km) in orbit around the Sun (expected launch date 2034). The signal is expected to be so strong that it will dominate the instrumental noise at low frequencies, forming a gravitational-wave “foreground” that will have to be contended with when searching for other gravitational sources in the LISA band.

At lower frequencies between $\sim 10^{-9}$ Hz and 10^{-7} Hz (corresponding to periods of order decades to years), pulsar timing arrays can be used to search for the GWB produced by the inspiral and merger of supermassive black-holes (SMBHs) in the centers of distant galaxies. A pulsar timing array basically functions as a galactic-scale gravitational-wave detector, with the radio pulses emitted by each pulsar behaving like ‘ticks’ of an extremely stable clock. By carefully monitoring the arrival times of these pulses, one can search for a GWB by looking for correlated modulations in the arrival times induced by a passing gravitational wave.

In addition to these *astrophysical* GWBs associated with stellar-mass or supermassive BHs and NSs, one also expects backgrounds of *cosmological* origin, produced in the very early universe, much before the formation of stars and galaxies. Two examples, indicated in Figure 5, are cosmic strings (line-like defects associated with phase transistions in the early universe) and relic gravitational waves (quantum fluctuations in the geometry of space-time, driven to macroscopic scales by a period of rapid expansion—e.g., inflation—a mere $\sim 10^{-32}$ s after the Big Bang). This relic background is potentially detectable by its effect on the polarization of the CMB radiation. The Planck satellite and BICEP experiment (located at the South Pole) are searching for this signal.

2.2 Different signal properties

Not surprisingly, different sources of a GWB give rise, in general, to different properties of the observed signal. These differences are what will allow us to infer the source of the background from the measured signal. For example:

(i) Stochastic backgrounds can differ from one another in terms of the angular distribution of gravitational-wave power on the sky. Cosmologically-generated backgrounds, like those from cosmic strings or relic gravitational waves, are expected to be statistically *isotropic*, with equal gravitational-wave power in all different directions, similar to the CMB (Figure 1). Different statistically isotropic backgrounds will be characterized by different angular power spectra, C_l as a

function of multipole moment l , where

$$C(\theta) = \sum_{l=0}^{\infty} \frac{2l+1}{4\pi} C_l P_l(\cos \theta), \quad (2.1)$$

is the angular correlation between the gravitational-wave power coming from two directions \hat{n} and \hat{n}' separated by angle θ . Statistically isotropic backgrounds are to be contrasted with *anisotropic* backgrounds, whose distribution of power on the sky follows the spatial distribution of sources. For example, the “confusion-limited” foreground that LISA will see from the population of close white-dwarf binaries in the Milky Way will have its gravitational-wave power concentrated in the direction of the Milky Way. Figure ?? shows simulated skymaps for a statistically isotropic background (left panel) and an anisotropic background (right panel). The anisotropic background in that figure follows the galactic plane in equatorial coordinates.

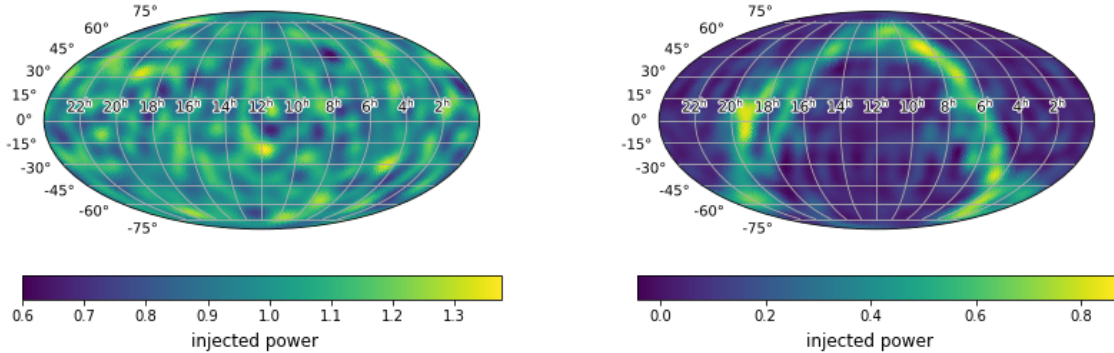


Figure 5: Simulated sky maps of gravitational-wave power for a statistically isotropic background (left panel) and an anisotropic background (right panel).

(ii) Stochastic backgrounds can also differ in temporal distribution and amplitude. We have already seen examples of this in Figure 2, for the expected backgrounds from stellar-mass BBH mergers and BNS mergers throughout the universe (a LIGO source). As mentioned earlier, the rate estimates and durations of these individual merger signals are such that the BBH background is expected to be popcorn-like (consisting of non-overlapping mergers), while that for the BNS background is expected to be stationary and confusion-limited (consisting of several overlapping BNS mergers at any instant of time). Another example of non-trivial temporal dependence is the confusion-limited signal from close white-dwarf binaries in the Milky Way (a LISA source). This is an amplitude-modulated signal with a 6-month period (Figure 6), due to LISA’s “cartwheeling” orbital motion around the Sun. (The antenna pattern of LISA will point in the direction of the Galactic center twice every year.) From the figure, we also see that the expected white-dwarf binary signal will be larger than that of the instrumental noise for LISA, thus constituting an astrophysical *foreground*. This is atypical, however, as most expected GWBs will sit below the instrumental noise (e.g., for advanced LIGO / Virgo, pulsar timing, CMB polarization experiments), requiring observation over long periods of time to confidently detect.

(iii) Stochastic backgrounds can also differ in their power spectra as shown in Figure 7. Here we plot simulated time-domain data (including the signals for an individual BNS merger and BBH ringdown²), histograms, and power spectra for three different types of GWBs. For these toy-model

²Our toy-model simulation for BBH ringdown is simply a damped sinusoid with frequency 440 Hz. It has the correct qualitative behavior for a BBH ringdown, but is not meant to be astrophysically realistic.

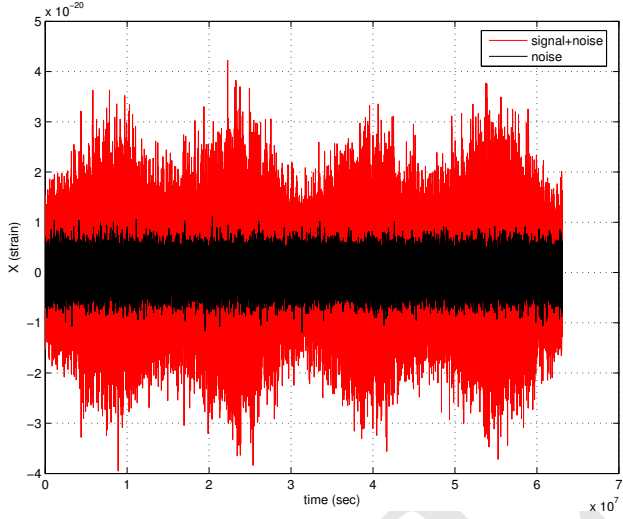


Figure 6: Simulated time-domain output of a particular combination of the LISA data over a 2-year period. The modulation of the signal with a 6-month period is apparent in the data. Figure taken from [1].

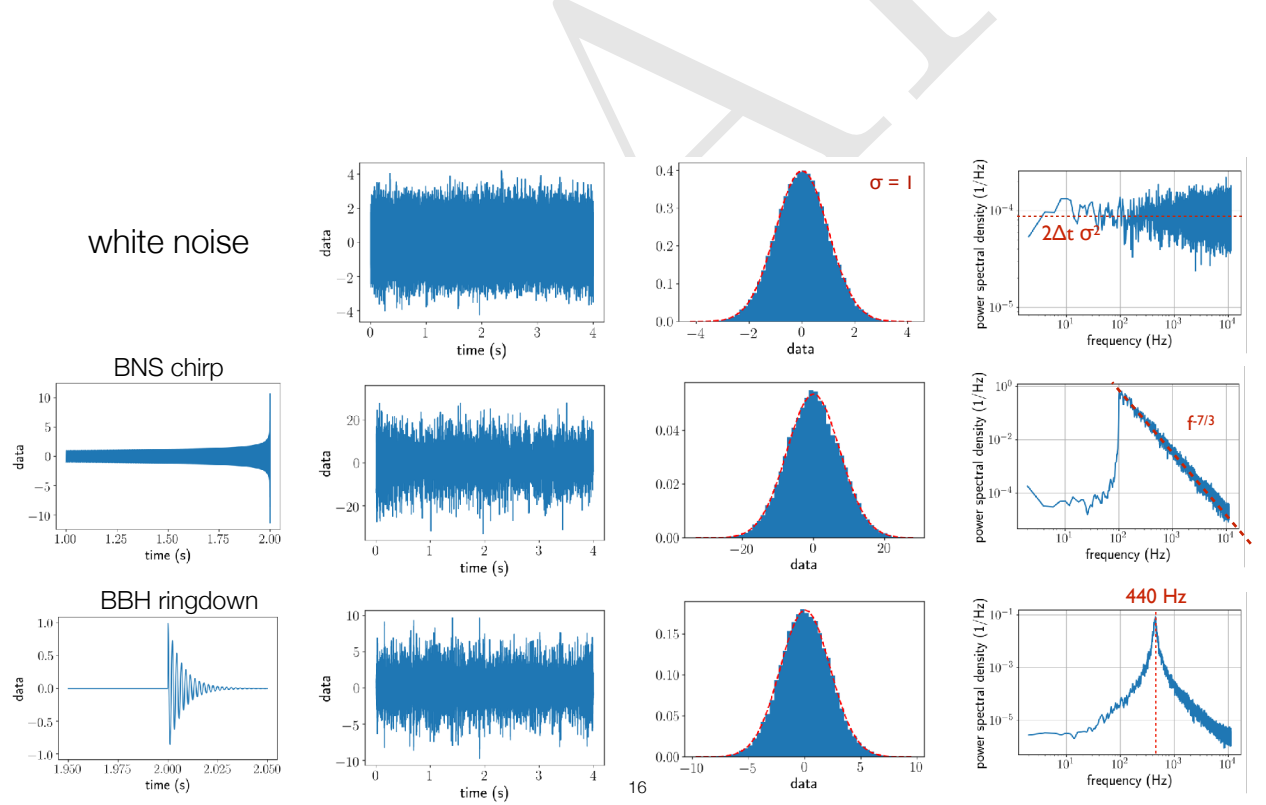


Figure 7: Simulated time-domain data (including the signals for an individual BNS merger and BBH ringdown), histograms, and power spectra for three different types of Gaussian-stationary GWBs.

simulations, we overlapped a sufficient number of individual BNS merger and BBH ringdown signals to produce Gaussian-stationary confusion-limited GWBs (second column and third columns). The difference between these backgrounds shows up in their power spectra (third column). The power spectra for the BNS merger and BBH ringdown backgrounds have the same shape as those for an individual BNS merger or BBH ringdown, scaled by the total number of sources contributing to the background.

3 Mathematical characterization of a stochastic background

Since the individual signals comprising a GWB background are either too weak or too numerous to individually detect, the combined signal for the background is for all practical purposes *random*, similar to noise in a single detector. Hence, we need to describe the GWB *statistically*, in terms of moments (i.e., ensemble averages) of the metric perturbations describing the GWB.

3.1 Ensemble averages and the energy density spectrum in GWs

Recall that gravitational waves are time-varying perturbations to the geometry of space-time, which propagate away from the source at the speed of light. In so-called transverse-traceless coordinates $(t, \vec{x}) \equiv (t, x^a)$, where $a = 1, 2, 3$, the metric perturbations corresponding to a plane wave (propagating in direction $\hat{k} \equiv -\hat{n}$) have two degrees of freedom, corresponding to the amplitudes of the plus (+) and cross (\times) polarizations of the gravitational wave (Figure 8). The metric perturbation

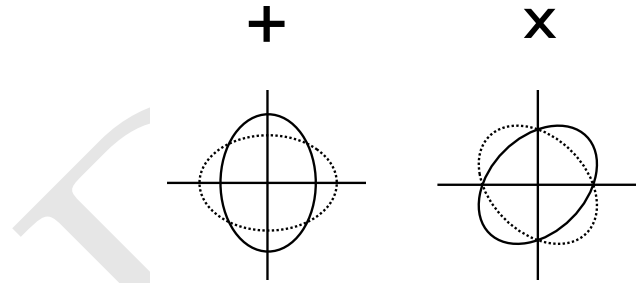


Figure 8: The two orthogonal polarizations of a gravitational wave.

for the most general GWB can thus be written as a superposition of such wave:

$$h_{ab}(t, \vec{x}) = \int_{-\infty}^{\infty} df \int d^2\Omega_{\hat{n}} \sum_{A=+, \times} h_A(f, \hat{n}) e_{ab}^A(\hat{n}) e^{i2\pi f(t + \hat{n} \cdot \vec{x}/c)} \quad (3.1)$$

where f denotes the frequency of the component waves, \hat{n} their direction on the sky, and $A = +, \times$ their polarization. The quantities $e_{ab}^A(\hat{n})$ are polarization tensors, given by

$$\begin{aligned} e_{ab}^+(\hat{n}) &= \hat{l}_a \hat{l}_b - \hat{m}_a \hat{m}_b, \\ e_{ab}^\times(\hat{n}) &= \hat{l}_a \hat{m}_b + \hat{m}_a \hat{l}_b, \end{aligned} \quad (3.2)$$

where \hat{l}, \hat{m} are any two orthogonal unit vectors in the plane orthogonal to \hat{n} (Figure ??). Typically, for stochastic background analyses, we take \hat{l}, \hat{m} to be the standard angular unit vectors tangent

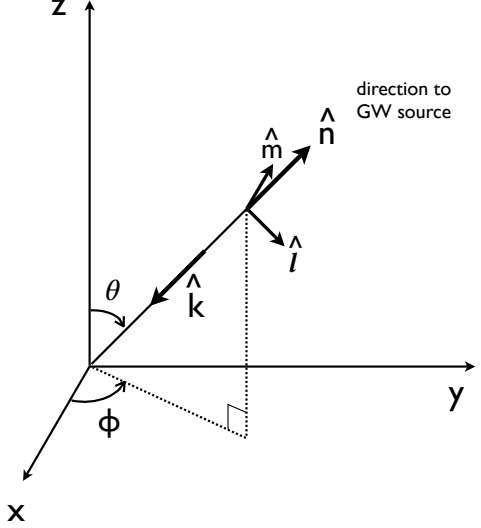


Figure 9: Coordinate system and unit vectors used in the plane-wave expansion of a GWB.

to the sphere:

$$\begin{aligned}\hat{n} &= \sin \theta \cos \phi \hat{x} + \sin \theta \sin \phi \hat{y} + \cos \theta \hat{z} \equiv \hat{r}, \\ \hat{l} &= \cos \theta \cos \phi \hat{x} + \cos \theta \sin \phi \hat{y} - \sin \theta \hat{z} \equiv \hat{\theta}, \\ \hat{m} &= -\sin \phi \hat{x} + \cos \phi \hat{y} \equiv \hat{\phi}.\end{aligned}\quad (3.3)$$

The quantities $h_A(f, \hat{n})$ are the Fourier coefficients of the plane wave expansion. Since, for a stochastic background, the metric perturbations $h_{ab}(t, \vec{x})$ are random variables, so to are the Fourier coefficients $h_A(f, \hat{n})$. The probability distributions of $h_A(f, \hat{n})$ define the statistical properties of the background.

Without loss of generality

3.2 Calculating $\Omega_{\text{gw}}(f)$ for an astrophysically-generated background

4 Correlation methods - basic idea

5 Some simple examples

We now apply the above correlation method

6 Non-trivial detector response

7 Non-trivial correlations

8 What to do in the absence of correlations?

9 Searching for the background of binary black-hole mergers

10 Exercises

A more detailed description of the suggested exercises.

1. Rate estimate of stellar-mass binary black hole mergers:

Estimate the total rate (number of events per time) of stellar-mass binary black hole mergers throughout the universe by multiplying LIGO's O1 local rate estimate $R_0 \sim 10 - 200 \text{ Gpc}^{-3} \text{ yr}^{-1}$ by the comoving volume out to some large redshift, e.g., $z = 10$. (For this calculation you can ignore any dependence of the rate density with redshift.) You should find a merger rate of ~ 1 per minute to a few per hour.

Hint: You will need to do numerically evaluate the following integral for proper distance today as a function of source redshift:

$$d_0(z) = \frac{c}{H_0} \int_0^z \frac{dz'}{E(z')} , \quad E(z) \equiv \sqrt{\Omega_m(1+z)^3 + \Omega_\Lambda} , \quad (10.1)$$

with

$$\Omega_m = 0.31 , \quad \Omega_\Lambda = 0.69 , \quad H_0 = 68 \text{ km s}^{-1} \text{ Mpc}^{-1} . \quad (10.2)$$

Doing that integral, you should find what's shown in Figure 10, which you can then evaluate at $z = 10$ to convert R_0 (number of events per comoving volume per time) to total rate (number of events per time) for sources out to redshift $z = 10$.

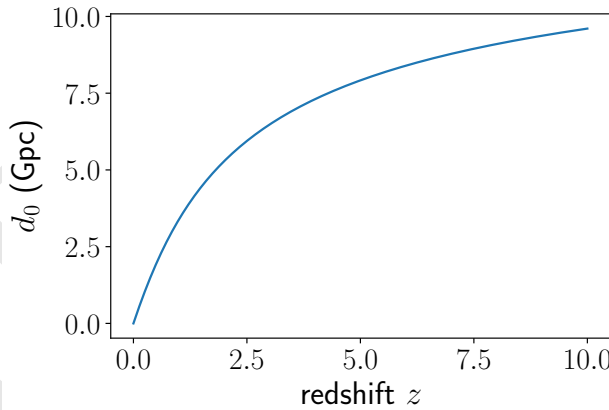


Figure 10

2. Relating $S_h(f)$ and $\Omega_{\text{gw}}(f)$:

Derive the relationship

$$S_h(f) = \frac{3H_0^2}{2\pi^2} \frac{\Omega_{\text{gw}}(f)}{f^3} \quad (10.3)$$

between the strain power spectral density $S_h(f)$ and the dimensionless fractional energy density spectrum $\Omega_{\text{gw}}(f)$. (*Hint:* You will need to use the various definitions of these quantities and also

$$\rho_{\text{gw}} = \frac{c^2}{32\pi G} \langle \dot{h}_{ab}(t, \vec{x}) \dot{h}^{ab}(t, \vec{x}) \rangle , \quad (10.4)$$

which expresses the energy-density in gravitational-waves to the metric perturbations $h_{ab}(t, \vec{x})$.)

3. Cosmology and the “Phinney formula” for astrophysical backgrounds:

(a) Using the Friedmann equation

$$\left(\frac{\dot{a}}{a}\right)^2 = H_0^2 \left(\frac{\Omega_m}{a^3} + \Omega_\Lambda \right) \quad (10.5)$$

for a spatially-flat FRW spacetime with matter and cosmological constant, and the relationship

$$1+z = \frac{1}{a(t)}, \quad a(t_0) \equiv 1 \quad (t_0 \equiv \text{today}), \quad (10.6)$$

between redshift z and scale factor $a(t)$, derive

$$\frac{dt}{dz} = -\frac{1}{(1+z)H_0E(z)}, \quad E(z) = \sqrt{\Omega_m(1+z)^3 + \Omega_\Lambda}. \quad (10.7)$$

(b) Using this result for dt/dz , show that

$$\Omega_{\text{gw}}(f) = \frac{f}{\rho_c H_0} \int_0^\infty dz R(z) \frac{1}{(1+z)E(z)} \left(\frac{dE_{\text{gw}}}{df_s} \right) \Big|_{f_s=f(1+z)} \quad (10.8)$$

in terms of the rate density $R(z)$ as measured in the source frame (number of events per comoving volume per time interval in the source frame). (*Hint:* The expression for dt/dz from part (a) will allow you to go from the “Phinney formula” for $\Omega_{\text{gw}}(f)$ written in terms of the number density $n(z)$,

$$\Omega_{\text{gw}}(f) = \frac{1}{\rho_c} \int_0^\infty dz n(z) \frac{1}{1+z} \left(f_s \frac{dE_{\text{gw}}}{df_s} \right) \Big|_{f_s=f(1+z)}, \quad (10.9)$$

to one in terms of the rate density $R(z)$, where $n(z) dz = R(z) |dt|_{t=t(z)}$. Note: Both of the above expressions for $\Omega_{\text{gw}}(f)$ assume that there is only one type of source, described by some set of average source parameters. If there is more than one type of source, one must sum the contributions of each source to $\Omega_{\text{gw}}(f)$.)

4. Optimal filtering for the cross-correlation statistic:

Verify the form

$$\tilde{Q}(f) \propto \frac{\Gamma_{12}(f)H(f)}{P_1(f)P_2(f)}, \quad (10.10)$$

of the optimal filter function in the weak-signal limit, where $H(f)$ is the assumed spectral shape of the gravitational-wave background, $\Gamma_{12}(f)$ is the overlap function, and $P_1(f)$, $P_2(f)$ are the power spectral densities of the outputs of the two detectors (which are approximately equal to $P_{n_1}(f)$, $P_{n_2}(f)$, respectively). Recall that the optimal filter $\tilde{Q}(f)$ maximizes the signal-to-noise ratio of the cross-correlation statistic. (*Hint:* Introduce an inner product on the space of functions of frequency $A(f)$, $B(f)$:

$$(A, B) \equiv \int df A(f)B^*(f)P_1(f)P_2(f). \quad (10.11)$$

This inner product has all of the properties of the familiar dot product of vectors in 3-dimensional space. The signal-to-noise ratio of the cross-correlation statistic can be written in terms of this inner product.)

5. Maximum-likelihood estimators for single and multiple parameters:

- (a) Show that the maximum-likelihood estimator \hat{a} of the single parameter a in the likelihood function

$$p(d|a, \sigma) \propto \exp \left[-\frac{1}{2} \sum_{i=1}^N \frac{(d_i - a)^2}{\sigma_i^2} \right] \quad (10.12)$$

is given by the noise-weighted average

$$\hat{a} = \sum_i \frac{d_i}{\sigma_i^2} / \sum_j \frac{1}{\sigma_j^2}. \quad (10.13)$$

- (b) Extend the previous calculation to the likelihood

$$p(d|A, C) \propto \exp \left[-\frac{1}{2} (d - MA)^\dagger C^{-1} (d - MA) \right], \quad (10.14)$$

where $A \equiv A_\alpha$ is a vector of parameters, $C \equiv C_{ij}$ is the noise covariance matrix, and $M \equiv M_{i\alpha}$ is the response matrix mapping A_α to data samples, $MA \equiv \sum_\alpha M_{i\alpha} A_\alpha$. For this more general case you should find:

$$\hat{A} = F^{-1}X, \quad (10.15)$$

where

$$F \equiv M^\dagger C^{-1} M, \quad X \equiv M^\dagger C^{-1} d. \quad (10.16)$$

In general, the matrix F (called the *Fisher* matrix) is not invertible, so some sort of regularization is needed to do the matrix inversion.

6. Timing-residual response for a 1-arm, 1-way detector:

Derive the timing residual response function

$$R^A(f, \hat{n}) = \frac{1}{2} u^a u^b e_{ab}^A(\hat{n}) \frac{1}{i2\pi f} \frac{1}{1 + \hat{n} \cdot \hat{u}} \left[1 - e^{-\frac{i2\pi f L}{c}(1 + \hat{n} \cdot \hat{u})} \right] \quad (10.17)$$

for a single-link (i.e., a one-arm, one-way detector like that for pulsar timing). Here \hat{u} is the direction of propagation of the electromagnetic pulse, and \hat{n} is the direction to the GW source (the direction of wave propagation is $\hat{k} \equiv -\hat{n}$ and the direction to the pulsar is $\hat{p} \equiv -\hat{u}$). The origin of coordinates is taken to be at the position of the detector.

7. Overlap function for colocated electric dipole antennae:

Show that the overlap function for a pair of (short) colocated electric dipole antennae pointing in directions \hat{u}_1 and \hat{u}_2 is given by

$$\Gamma_{12} \propto \hat{u}_1 \cdot \hat{u}_2 \equiv \cos \zeta \quad (10.18)$$

for the case of an unpolarized, isotropic electromagnetic field. (*Hint:* “short” means that the phase of the electric field can be taken to be constant over of the lengths of the dipole antennae, so that the response of antenna $I = 1, 2$ to the field is given by $r_I(t) = \hat{u}_I \cdot \vec{E}(t, \vec{x}_0)$, where \vec{x}_0 is the common location of the two antenna.)

8. Maximum-likelihood estimators for the standard cross-correlation statistic:

Verify that

$$\hat{C}_{11} \equiv \frac{1}{N} \sum_{i=1}^N d_{1i}^2, \quad \hat{C}_{22} \equiv \frac{1}{N} \sum_{i=1}^N d_{2i}^2, \quad \hat{C}_{12} \equiv \frac{1}{N} \sum_{i=1}^N d_{1i}d_{2i} \quad (10.19)$$

are maximum-likelihood estimators of

$$S_1 \equiv S_{n_1} + S_h, \quad S_2 \equiv S_{n_2} + S_h, \quad S_h, \quad (10.20)$$

for the case of N samples of a white GWB in uncorrelated white detector noise, for a pair of colocated and coaligned detectors. Recall that the likelihood function is

$$p(d|S_{n_1}, S_{n_2}, S_h) = \frac{1}{\sqrt{\det(2\pi C)}} \exp \left[-\frac{1}{2} d^T C^{-1} d \right], \quad (10.21)$$

where

$$C = \begin{bmatrix} (S_{n_1} + S_h) \mathbf{1}_{N \times N} & S_h \mathbf{1}_{N \times N} \\ S_h \mathbf{1}_{N \times N} & (S_{n_2} + S_h) \mathbf{1}_{N \times N} \end{bmatrix} \quad (10.22)$$

and

$$d^T C^{-1} d \equiv \sum_{I,J=1}^2 \sum_{i,j=1}^N d_{Ii} (C^{-1})_{Ii, Jj} d_{Jj}. \quad (10.23)$$

9. Derivation of the maximum-likelihood ratio detection statistic:

Verify that twice the log of the maximum-likelihood ratio for the standard stochastic likelihood function goes like the square of the (power) signal-to-noise ratio,

$$2 \ln \Lambda_{\text{ML}}(d) \simeq \frac{\hat{C}_{12}^2}{\hat{C}_{11} \hat{C}_{22}/N}, \quad (10.24)$$

in the weak-signal approximation. (*Hint:* For simplicity, do the calculation in the context of N samples of a white GWB in uncorrelated white detector noise, for a pair of colocated and coaligned detectors, using the results of Exercise 8.)

10. Standard cross-correlation likelihood by marginalizing over stochastic signal prior:

Derive the standard form of the likelihood function for stochastic background searches

$$p(d|S_{n_1}, S_{n_2}, S_h) = \frac{1}{\sqrt{\det(2\pi C)}} \exp \left[-\frac{1}{2} \sum_{I,J=1}^2 d_I (C^{-1})_{IJ} d_J \right], \quad (10.25)$$

where

$$C \equiv \begin{bmatrix} S_{n_1} + S_h & S_h \\ S_h & S_{n_2} + S_h \end{bmatrix}, \quad (10.26)$$

by marginalizing

$$p_n(d - h|S_{n_1}, S_{n_2}) = \frac{1}{2\pi\sqrt{S_{n_1}S_{n_2}}} \exp \left[-\frac{1}{2} \left\{ \frac{(d_1 - h)^2}{S_{n_1}} + \frac{(d_2 - h)^2}{S_{n_2}} \right\} \right] \quad (10.27)$$

over the signal samples h for the *stochastic* signal prior

$$p(h|S_h) = \frac{1}{\sqrt{2\pi S_h}} \exp\left[-\frac{1}{2} \frac{h^2}{S_h}\right]. \quad (10.28)$$

In other words, show that

$$p(d|S_{n_1}, S_{n_2}, S_h) = \int_{-\infty}^{\infty} dh p_n(d - h|S_{n_1}, S_{n_2}) p(h|S_h). \quad (10.29)$$

(*Hint:* You'll have to complete the square in the argument of the exponential in the marginalization integral.)

References

- [1] Romano, Joseph D. and Cornish, Neil. J., “Detection methods for stochastic gravitational-wave backgrounds: a unified treatment”, *Living Reviews in Relativity*, **20**(1), 2 (Apr 04, 2017). [DOI]URL:
<https://doi.org/10.1007/s41114-017-0004-1>.
- [2] Smith, Rory and Thrane, Eric, “Optimal Search for an Astrophysical Gravitational-Wave Background”, *Phys. Rev. X*, **8**, 021019 (Apr 2018). [DOI]URL:
<https://link.aps.org/doi/10.1103/PhysRevX.8.021019>.